


RESEARCH ARTICLE

Comparisons of Quantitative Parameters of Ga-68-Labelled Fibroblast Activating Protein Inhibitor (FAPI) PET/CT and [¹⁸F]F-FDG PET/CT in Patients with Liver Malignancies

Dheeratama Siripongsatian¹, Chetsadaporn Promteangtrong¹, Anchisa Kunawudhi¹, Peerapon Kiatkittikul¹, Natphimol Boonkawin¹, Chatchawarin Chinnanthachai¹, Attapon Jantarato¹, and Chanisa Chotipanich¹

¹National Cyclotron and PET Centre Building, Chulabhorn Hospital, 54 Kamphangpetch 6 Road, Talad Bangkhen, Laksi, Bangkok 10210, Thailand 2022

Abstract

Purpose: To compare quantitative parameters and tumour detection rates of [⁶⁸Ga]Ga-FAPI PET/CT with those of dedicated liver PET/MRI and ¹⁸F-FDG PET in patients with liver malignancies.

Procedures: Twenty-seven patients (29 imaging studies) with diagnosed or suspected liver malignancies who underwent [⁶⁸Ga]Ga-FAPI-46 PET/CT, liver PET/MRI, and [¹⁸F]FDG PET/CT between September 2020 and June 2021 were retrospectively analysed. MRI findings were used as the reference standard for diagnosis.

Results: The 27 patients had a median age of 68 years (interquartile range: 60–74 years; 21 men). Primary intrahepatic tumours were reported in 13 patients (15 imaging studies) with cholangiocarcinoma (CCA) and in 14 patients with hepatocellular carcinoma (HCC). All intrahepatic lesions detectable on MRI were also detected on [⁶⁸Ga]Ga-FAPI-46 PET/CT giving a sensitivity of 100% (19/19), whereas the sensitivity of [¹⁸F]FDG PET/CT was 58% (11/19). All intrahepatic lesions were detected on [⁶⁸Ga]Ga-FAPI-46 PET/CT, on which they showed higher activity (median SUV_{max}: 15.61 vs. 5.17; $P < .001$) and higher target-to-background ratio (TBR; median, 15.90 vs. 1.69, $P < .001$) than on [¹⁸F]FDG, especially in patients with CCA (median TBR, 21.08 vs. 1.47, respectively; $P < .001$). The uptake positivity rate in regional node metastasis was 100% (12/12) on [⁶⁸Ga]Ga-FAPI-46 PET/CT compared with 58% (7/12) on [¹⁸F]FDG PET/CT. All patients with distant metastasis (100%, 14/14) were detected on both [¹⁸F]FDG and [⁶⁸Ga]Ga-FAPI-46 PET/CT imaging, although more distant metastatic lesions were detected on [⁶⁸Ga]Ga-FAPI-46 PET/CT than on [¹⁸F]FDG (96% (42/44) vs. 89% (39/44), respectively).

Conclusion: [⁶⁸Ga]Ga-FAPI PET/CT with dedicated liver PET/MRI shows potential for superior detection of hepatic malignancy compared with [¹⁸F]FDG PET/CT or MRI alone.

Key words PET/CT · PET/MRI · Cancer-associated fibroblasts · Fibroblast activation protein · Fluorodeoxyglucose · Hepatocellular carcinoma · Cholangiocarcinoma

Introduction

Liver cancer is the third most common cause of cancer-related death worldwide [1]. Primary liver cancer consists of two major histological subtypes: hepatocellular carcinoma (HCC) and cholangiocarcinoma (CCA). In Thailand, primary liver cancer is the leading cancer in men, but in contrast to other countries, cholangiocarcinoma is the predominant subtype of liver cancer, rather than HCC [2]. The high mortality rate of liver cancer indicates the inefficiency of current strategies for evaluating and treating it [3]. Imaging plays an important role in diagnosis, initial staging, evaluation of treatment response, and detection of recurrence. While magnetic resonance imaging (MRI) has significantly better sensitivity for detecting HCC than contrast-enhanced computed tomography, there is no significant difference in specificity between the two modalities [4]. Currently, fluorine-18 fluoro-2-deoxyglucose ([¹⁸F]FDG) positron emission tomography (PET)/CT is increasingly being recognised as an effective diagnostic imaging tool for cancer. Variable FDG uptake in HCC is related to the differentiation of the tumour. The sensitivity of [¹⁸F]FDG PET for moderately or poorly differentiated HCC is greater than that for well-differentiated or low-grade tumours [5, 6]. The sensitivity of [¹⁸F]FDG PET/CT ranges from 50 to 70% for HCC, similar to that of CT and MRI [5–7]. [¹⁸F]FDG PET has comparable diagnostic accuracy to MRI with respect to the tumour T stage. The reported pooled sensitivity and specificity of FDG PET/CT for tumour T stage are 91% and 85%, respectively, values that compare very closely with those of MRI, at 90% and 84%, respectively. However, data regarding regional node metastasis and N stage are limited owing to the unsatisfactory diagnostic accuracy of both imaging modalities. Furthermore, [¹⁸F]FDG PET/CT has low sensitivity but high specificity for detecting distant metastasis, with reported pooled sensitivity and specificity of 56% and 95%, respectively [8]. Gallium (Ga)68-labelled fibroblast activating protein inhibitor (FAPI) was developed to evaluate fibroblast activation in oncological imaging, with fibroblast activating proteins being highly expressed in cancer-associated fibroblasts in various epithelial carcinomas. The significantly lower hepatic background uptake of [⁶⁸Ga]Ga-FAPI in comparison with that of [¹⁸F]FDG is also an important factor improving the sensitivity of [⁶⁸Ga]Ga-FAPI for liver tumour detection in comparison with [¹⁸F]FDG PET [9, 10]. Previous studies showed that [⁶⁸Ga]Ga-FAPI PET/CT has better sensitivity than [¹⁸F]FDG PET/CT for detecting liver malignancies [11, 12].

This study aimed to compare the quantitative parameters and tumour detection rates of dedicated liver PET/MRI and [¹⁸F]FDG PET/CT in patients with liver malignancies.

Materials and Methods

Patients

This retrospective study was approved by the Human Research Ethics Committee of Chulabhorn Research

Institute. Patients diagnosed with or suspected to have liver malignancies between September 2020 and June 2021 were enrolled. Twenty-seven patients (29 imaging studies) were included, and all underwent both [⁶⁸Ga]Ga-FAPI-46 PET/CT with liver PET/MRI and [¹⁸F]FDG PET/CT at our centre. All patients underwent both PET/CT scans within 7 days.

Radiopharmaceuticals

[¹⁸F]FDG was manufactured using an automated synthesis module (TracerLab MXfdg; GE Healthcare) with a sterile cassette and reagents (ABX Advanced Biomedical Compounds). [⁶⁸Ga]Ga-FAPI-46 was synthesised using an iTG 68 germanium (Ge)/[⁶⁸Ga]Ga generator and an automated module (iQS-TS; Isotope Technologies Garching GmbH, Munich, Germany) in a good manufacturing practice (GMP)-compliant process, as previously described [13–15] (with some modifications). The radiochemical purities of the [¹⁸F]FDG and [⁶⁸Ga]Ga-FAPI-46 solution were >95%. All quality control parameters for both radiotracers conformed to the limits prescribed by the European Pharmacopoeia.

[⁶⁸Ga]Ga-FAPI PET/CT with Dedicated Liver PET/MRI Imaging

[⁶⁸Ga]Ga-FAPI-46 PET imaging was performed on a 64-slice Siemens Biograph vision scanner (Siemens Healthineers, Erlangen, Germany) after intravenous injection of 2.59 MBq/kg of [⁶⁸Ga]Ga-FAPI-46 over approximately 60 min. Non-contrast-enhanced CT was also acquired for attenuation correction (kV = 120, effective mAs = 25, Care Dose 4D, quality reference = 70).

PET was acquired in the three-dimensional (3D) list mode using continuous bed motion with the patient in a headfirst supine position. The speed was set at 1.6–1.8 mm/s. All PET data were reconstructed using True X+ TOF (Ultra HD PET) with iteration number = 2 and subsets = 5. Scatter and decay correction were also performed.

After PET/CT scanning, dedicated liver PET/MRI was performed on an integrated 3.0-Tesla Siemens Biograph mMR scanner (Siemens Healthcare GmbH). A single-bed PET dynamic list mode acquisition was acquired simultaneously with the MRI acquisition. A Dixon high-resolution abdominal sequence with echo time (TE) = 1.28/2.51 ms and repetition time (TR) = 4.14 ms was acquired, which was subjected to five-compartment segmentation (air, water, lung, adipose tissue, bone) postprocessing for the model reference adaptive control (MRAC) sequence. Further MRI sequences acquired were coronal T2-weighted, axial T2-weighted, fat-suppressed axial T2-weighted, axial diffusion-weighted (DWI) with *b* = 50, 500, and 1000, and an axial T1-weighted (T1W) volumetric interpolated breath-hold examination (VIBE) performed prior to gadolinium enhancement. Abdominal dynamic contrast-enhanced MRI was performed with Dotarem in patients with cholangiocarcinoma (CCA)

and with Primovist in patients with HCC, using an injection rate of 2 ml/s. This was followed by an axial T1W VIBE sequence with fat suppression acquired at 30 s, 60 s, 90 s, and 5 min after Dotarem injection. Additional axial T1W VIBE fat-suppressed images were obtained at 10 and 20 min after the Primovist injection. Coronal fat-suppressed T1W VIBE images were also obtained.

[¹⁸F]FDG PET/CT Imaging

[¹⁸F]FDG PET/CT was performed approximately 60 min after intravenous injection of 2.59 MBq/kg of [¹⁸F]FDG using the same PET/CT scanner used for the [⁶⁸Ga]Ga-FAPI-46 imaging. All patients underwent both PET/CT scans within 1 week. The blood glucose concentration of all patients was < 200 mg/dl before [¹⁸F]FDG administration.

Image Analysis

All PET images were analysed using a Syngovia workstation (Siemens Healthineers) and were displayed in coronal, axial, and sagittal planes with rotating 3D images. The MRI dataset was analysed using the MR oncology workflow program of the Syngovia workstation. The acquired PET data were reconstructed using ordered subset expectation maximisation and a point spread function.

All PET/CT scans were interpreted independently by two experienced board-certified nuclear medicine physicians (with 5 and 10 years of experience) who were blinded to the patients' clinical information. On visual analysis, positive lesions were defined as those showing non-physiological focal tracer uptake on PET images. Three-dimensional regions of interest were drawn around the region of abnormal uptake on axial slices to obtain the quantitative parameters. The maximum standardised

uptake value (SUVmax) was automatically calculated to evaluate tracer uptake in primary tumours, lymph nodes, and distant metastases. The target-to-background ratio (TBR) of each primary tumour was calculated by dividing the SUVmax of the lesion by the SUVmean of normal background liver. MRI images from the dedicated liver PET/MRI were used as the reference standard, and PET/MRI images were used for coregistration of intrahepatic lesions. On MRI, positive lesions were considered according to their abnormal enhancing pattern and fluid restriction pattern.

Statistical Analysis

Semiquantitative parameters are described as median and interquartile range, and were compared using paired and unpaired *t*-tests, depending on the data characteristics. The MRI findings were used as the reference standard in the diagnostic performance calculations. Statistical significance was set at $P < 0.05$, and STATA software version 11 (StataCorp, College Station, TX, USA) was used for all analyses.

Results

Patients

This study included 27 patients (median age: 68 years; interquartile range [IQR]: 60–74 years; 21 men) diagnosed with or suspected of liver malignancies who underwent [⁶⁸Ga]Ga-FAPI-46 PET/CT with liver PET/MRI and [¹⁸F]FDG PET/CT between September 2020 and June 2021. Of the 27 patients, 13 were diagnosed with CCA and 14 with HCC according to typical findings on MRI and histopathology. Table 1 summarises the patients' demographic data. All patients underwent liver MRI according to the dedicated PET/MRI protocol.

Positivity of Intrahepatic Tumours

The uptake-positive rates of [¹⁸F]FDG and [⁶⁸Ga]Ga-FAPI-46 PET/CT imaging in all intrahepatic tumours were 52% (11/21) and 100% (21/21), respectively.

According to the reference standard MRI findings, two patients with HCC showed false-positive [⁶⁸Ga]Ga-FAPI-46 PET/CT findings, but no false positives were found in patients with CCA. All intrahepatic lesions detected on MRI were also detected on [⁶⁸Ga]Ga-FAPI-46 PET/CT (100%, 19/19). The sensitivity of [¹⁸F]FDG PET/CT was 58% (11/19).

All intrahepatic lesions showed higher activity (median SUVmax: 15.61 vs. 5.17; $P < 0.001$) and higher TBR (median, 15.90 vs. 1.69; $P < 0.001$) on [⁶⁸Ga]Ga-FAPI-46 PET/CT than on [¹⁸F]FDG PET/CT, with TBR showing a particularly large difference in patients with CCA (median TBR, 21.08 vs. 1.47; $P < 0.001$).

Table 1 Patient characteristics

<i>n</i> = 27	
Age (years)	68 (60–74)
Gender (M:F)	21:6
Clinical questions for PET	
Staging before treatment	6 (22%)
Restaging	18 (67%)
Suspected recurrence	3 (11%)
Treatment status	
Treatment-naïve	6 (22%)
Previous surgical procedure	11 (41%)
Previous systemic treatment	2 (7%)
Combined surgical procedure and systemic treatment	8 (30%)
Final diagnosis	
HCC	14 (52%)
CCA	13 (48%)

Values are median (interquartile range) or number (%)

Treatment-Naïve Patients

The histopathological results and typical radiographic findings on MRI were collected for the primary liver tumours of the treatment-naïve patients. Five out of six initially treatment-naïve patients had pathological confirmation. Another patient had the typical pattern of HCC following radiofrequency ablation treatment. Nonetheless, a decreased alpha fetoprotein (AFP) level was noted in clinical follow-up. In these treatment-naïve patients, the uptake-positive rates of [¹⁸F]FDG and [⁶⁸Ga]Ga-FAPI-46 in the primary lesions on PET/CT imaging were 67% (4/6) and 100% (6/6), respectively. Table 2 compares the positivity rates of intrahepatic lesions between [¹⁸F]FDG PET/CT and [⁶⁸Ga]Ga-FAPI PET/CT.

In the treatment-naïve patients, all primary lesions were detected with higher activity (median SUV_{max}: 22.21 vs. 8.66; $P < 0.001$) and higher TBR (median, 17.57 vs. 3.12; $P < 0.001$) on [⁶⁸Ga]Ga-FAPI-46 PET/CT than on [¹⁸F]FDG PET/CT, with TBR showing a particularly large difference in patients with CCA (median TBR, 21.07 vs. 3.12, respectively; $P < 0.001$) (Table 3). Figures 1 and 2 present representative cases.

When diagnostic performance was calculated using MRI as the reference standard, the sensitivities of [¹⁸F]FDG and [⁶⁸Ga]Ga-FAPI-46 PET/CT imaging for detecting intrahepatic lesions were 58% and 100%, respectively. For HCC, the sensitivities of [¹⁸F]FDG and [⁶⁸Ga]Ga-FAPI-46 PET/CT were 71% and 100%, respectively, while for CCA they were 50% and 100%, respectively.

The SUV_{max}, SUV_{mean}, SUV_{peak}, and TBR of [⁶⁸Ga]Ga-FAPI-46 were significantly higher in patients with CCA than in those with HCC ($P < 0.005$).

Table 2 Comparisons of the positivity rates of intrahepatic lesions on [¹⁸F]FDG and [⁶⁸Ga]Ga-FAPI-46 PET

Type of cancer	No. of studies	Positivity rate	
		[¹⁸ F]FDG PET/CT	[⁶⁸ Ga]Ga-FAPI-46 PET/CT
Naïve			
HCC	2	50% (1/2)	100% (2/2)
CCA	4	75% (3/4)	100% (4/4)
Total	6	67% (4/6)	100% (6/6)
Post-treatment			
HCC	12	57% (4/7)	100% (7/7)
CCA	11	38% (3/8)	100% (8/8)
Total	23	47% (7/15)	100% (15/15)
All studies			
HCC	14	56% (5/9)	100% (9/9)
CCA	15	50% (6/12)	100% (12/12)
Total	29	52% (11/21)	100% (21/21)

Local Recurrence and Residual Tumour (Post-treatment Subgroup)

Pathological confirmation was available for 2 of the 21 post-treatment patients. Because of the invasiveness of procedures required for pathological diagnosis, follow-up imaging and clinical results were used as the reference standard for the other patients. One post-treatment HCC patient died from respiratory failure due to COVID-19. The uptake-positive rates in local recurrence and residual tumour lesions were 46.7% (7/15) on [¹⁸F]FDG PET/CT and 100% (15/15) on [⁶⁸Ga]Ga-FAPI-46 PET/CT. All intrahepatic lesions were detected on [⁶⁸Ga]Ga-FAPI-46 PET/CT. In addition, the detection rate of intrahepatic lesions on [¹⁸F]FDG PET/CT was higher in patients with HCC (57%, 4/7) than in patients with CCA (38%, 3/8).

The typical pattern of FAPI uptake in post-surgical/post-treatment inflammation was diffuse uptake, especially in inflammation from radiotherapy or surgery, but areas of inflammation did not show as abnormal on MRI. Except for two patients with HCC who underwent transarterial chemoembolisation, the images showed abnormal focal (but not diffuse) FAPI uptake in the intrahepatic lesions, which MRI and follow-up CT confirmed as post-treatment change. According to the MRI findings, there were two false-positive lesions on [⁶⁸Ga]Ga-FAPI-46 PET/CT in patients with HCC. One false-positive lesion in a patient with HCC was false-positive on both [⁶⁸Ga]Ga-FAPI-46 PET/CT and [¹⁸F]FDG PET/CT. One lesion was 6.8 cm, with 2-month follow-up CECT showing a partial lipiodol-stained mass with peripheral rim uptake and stable size. The other lesion was 1.5 cm at 7-month follow-up and showed no progression according to imaging or tumour markers. Both were negative according to the enhancing pattern on MRI. All lesions identified on MRI were also identified on [⁶⁸Ga]Ga-FAPI-46 PET/CT (100%, 41/41), whereas a much lower number of lesions (detection rate: 39% [16/41]) were detected on [¹⁸F]FDG PET/CT. Figure 3 presents a representative case.

Regional Node Metastasis

The number of detected regional node metastases was higher in patients with CCA ($n = 10$ patients, 29 nodes) than in those with HCC ($n = 2$ patients, 2 nodes). The uptake-positive rates of regional node metastases were 100% (12/12) on [⁶⁸Ga]Ga-FAPI-46 PET/CT and 58% (7/12) on [¹⁸F]FDG PET/CT. Moreover, on [⁶⁸Ga]Ga-FAPI-46 PET/CT, nodal metastases were detected with higher activity (median SUV_{max}: 8.35 vs. 4.61; $P = 0.02$) and higher TBR (median, 4.51 vs. 2.28; $P < 0.001$) than on [¹⁸F]FDG PET/CT. The latest available follow-up data revealed one case of post-treatment CCA with false-positive FDG and FAPI-avid nodal metastases (a 0.5-cm intra-abdominal para-aortic node and a 0.6-cm mediastinal subaortic node).

Table 3 Comparisons of [¹⁸F]FDG and [⁶⁸Ga]Ga-FAPI-46 uptake in intrahepatic lesions

	HCC	CCA
Naïve		
No. of lesions	5	5
[¹⁸ F]FDG		
Tumour SUVmax	6.31 (3.37–9.86)	8.66 (4.17–23.23)
TBR	2.34 (1.25–3.67)	3.12 (1.62–7.74)
No. of positive lesions	1	3
[⁶⁸ Ga]Ga-FAPI-46		
Tumour SUVmax	7.54 (5.23–8.30)	24.02 (19.82–26.00)
TBR	4.98 (2.04–7.90)	21.07 (17.39–23.94)
No. of positive lesions	5	5
<i>P</i> values		
SUVmax on FAPI vs. SUVmax on FDG	0.419	0.013*
TBR on FAPI vs. TBR on FDG	0.096	0.001*
Post-treatment		
No. of lesions	9	26
[¹⁸ F]FDG		
Tumour SUVmax	5.38 (3.71–20.16)	4.81 (3–38–14.35)
TBR	1.84 (1.44–6.95)	1.42 (0.98–4.64)
No. of positive lesions	5	8
[⁶⁸ Ga]Ga-FAPI-46		
Tumour SUVmax	11.19 (4.98–18.89)	17.47 (5.27–30.25)
TBR	10.42 (4.65–13.54)	21.55 (3.59–35.18)
No. of positive lesions	9	26
<i>P</i> values		
SUVmax on FAPI vs. SUVmax on FDG	0.041*	<0.001*
TBR on FAPI vs. TBR on FDG	<0.001*	<0.001*
All studies		
No. of lesions	14	31
[¹⁸ F]FDG		
Tumour SUVmax	5.53 (3.37–23.23)	4.89 (3.38–23.23)
TBR	1.96 (1.25–6.95)	1.47 (0.98–7.74)
No. of positive lesions	6	11
[⁶⁸ Ga]Ga-FAPI-46		
Tumour SUVmax	9.65 (4.98–18.89)	19.82 (5.27–30.25)
TBR (median, range)	7.90 (2.03–13.54)	21.08 (3.59–35.18)
No. of positive lesions	14	31
<i>P</i> values		
SUVmax on FAPI vs. SUVmax on FDG	0.026*	<0.001*
TBR on FAPI vs. TBR on FDG	<0.001*	<0.001*

*Values are presented as median (range)

Distant Metastasis

Table 4 summarises the distant lymph node metastases and visceral metastases detected using [¹⁸F]FDG and [⁶⁸Ga]Ga-FAPI-46 PET/CT. [¹⁸F]FDG and [⁶⁸Ga]Ga-FAPI-46 PET/CT imaging detected all patients with distant metastasis (100%, 14/14), although more distant metastatic lesions were detected on [⁶⁸Ga]Ga-FAPI-46 PET/CT than on [¹⁸F]FDG (96% [42/44] vs. 89% [39/44], respectively), and four peritoneal metastases and one brain metastasis detected on [⁶⁸Ga]Ga-FAPI-46 PET were undetectable on [¹⁸F]FDG PET. There

were also two FDG-avid bone metastases in a patient with HCC that were not detected on [⁶⁸Ga]Ga-FAPI-46 PET, with [⁶⁸Ga]Ga-FAPI-46 PET showing low SUVmax and TBR. However, 2-month follow-up with whole abdominal CT revealed progression of these bone metastases with obvious mass-forming lesions.

Compared with [¹⁸F]FDG, [⁶⁸Ga]Ga-FAPI-46 PET/CT showed higher activity and clearer tumour delineation in distant metastases, especially peritoneal (median SUVmax, 17.23 vs. 7.44, *P* = 0.016; median TBR, 14.69 vs. 3.52, *P* = 0.008) and brain metastasis (SUVmax, 25.30 vs. 8.86;

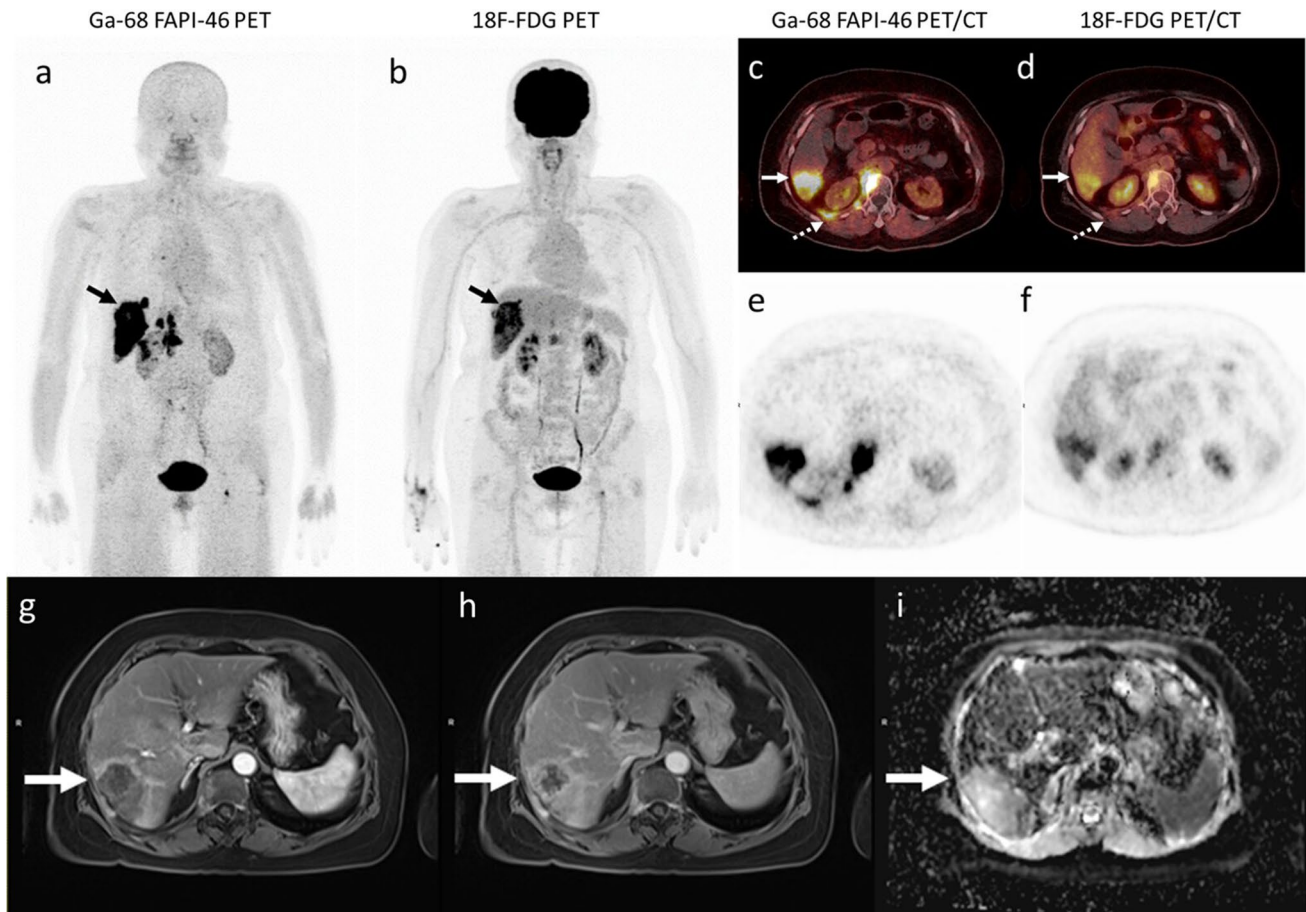


Fig. 1. A 62-year-old woman with intrahepatic cholangiocarcinoma underwent PET/CT with dedicated liver PET/MRI for initial staging. (a) MIP image of [⁶⁸Ga]Ga-FAPI-46 PET, (c) fused axial [⁶⁸Ga]Ga-FAPI-46 PET/CT image, and (e) axial [⁶⁸Ga]Ga-FAPI-46 attenuation correction PET image show a lesion with intense uptake (SUV_{max}=24.02, TBR=21.07) in the liver (arrows) corresponding to the primary liver cancer. (b) MIP [¹⁸F]FDG PET image, (d) fused axial [¹⁸F]FDG PET/CT images, and (f) axial [¹⁸F]FDG PET attenuation-corrected PET image show less tracer uptake than [⁶⁸Ga]Ga-FAPI-46 PET (SUV_{max}=15.79, TBR=4.97) in the corresponding liver lesions (arrows). The corresponding axial MR images show a mass in hepatic segments VI/VII with adjacent intrahepatic bile duct dilatation. This lesion shows delayed enhancement (g, h) and restricted diffusion on (i) DWI/ADC images.

TBR, 194.60 vs. 1.16). Figure 4 presents a representative case.

Changes in Patient Management

All intrahepatic tumours were detected on [⁶⁸Ga]Ga-FAPI-46 PET/CT with dedicated liver PET/MRI, with this imaging protocol detecting lesions that were not detected on [¹⁸F]FDG PET/CT in 9 of 19 patients (47%; seven patients with residual disease or local recurrence and two treatment-naïve patients with primary liver malignancies). Additionally, lesions that were undetectable on [¹⁸F]FDG PET were detected on [⁶⁸Ga]Ga-FAPI-46 PET/CT in 4 of 12 patients (33%).

All patients with distant metastasis were detected on [¹⁸F]FDG and [⁶⁸Ga]Ga-FAPI-46 PET/CT imaging (100%, 14/14), but additional peritoneal metastases (four lesions) and a brain metastasis (one lesion) were also detected on [⁶⁸Ga]

Ga-FAPI-46 PET but not on [¹⁸F]FDG PET, with these additional detections affecting the patients' management, quality of life, and prognosis. Figure 5 presents a representative case.

Correlation of Quantitative Parameters

Apparent diffusion coefficient (ADC) values were obtained from the diffusion MRI. The median (IQR) ADC values of all intrahepatic tumours, CCA, and HCC were 0.73 (0.55–0.91), 0.74 (0.55–0.93), and 0.73×10^{-3} mm²/s (0.53–0.84), respectively. Spearman's rank correlation revealed moderate correlations ($\rho > 0.6$) between quantitative parameters of [⁶⁸Ga]Ga-FAPI-46 PET/CT (SUV_{max}, SUV_{mean}, SUV_{peak}, and TBR) and SUV values of [¹⁸F]FDG PET/CT (SUV_{max}, SUV_{mean}, and SUV_{peak}) in patients with CCA, with these correlations showing statistical significance ($p < 0.05$). However, the correlations between SUV values of [⁶⁸Ga]Ga-FAPI-46 PET/CT and

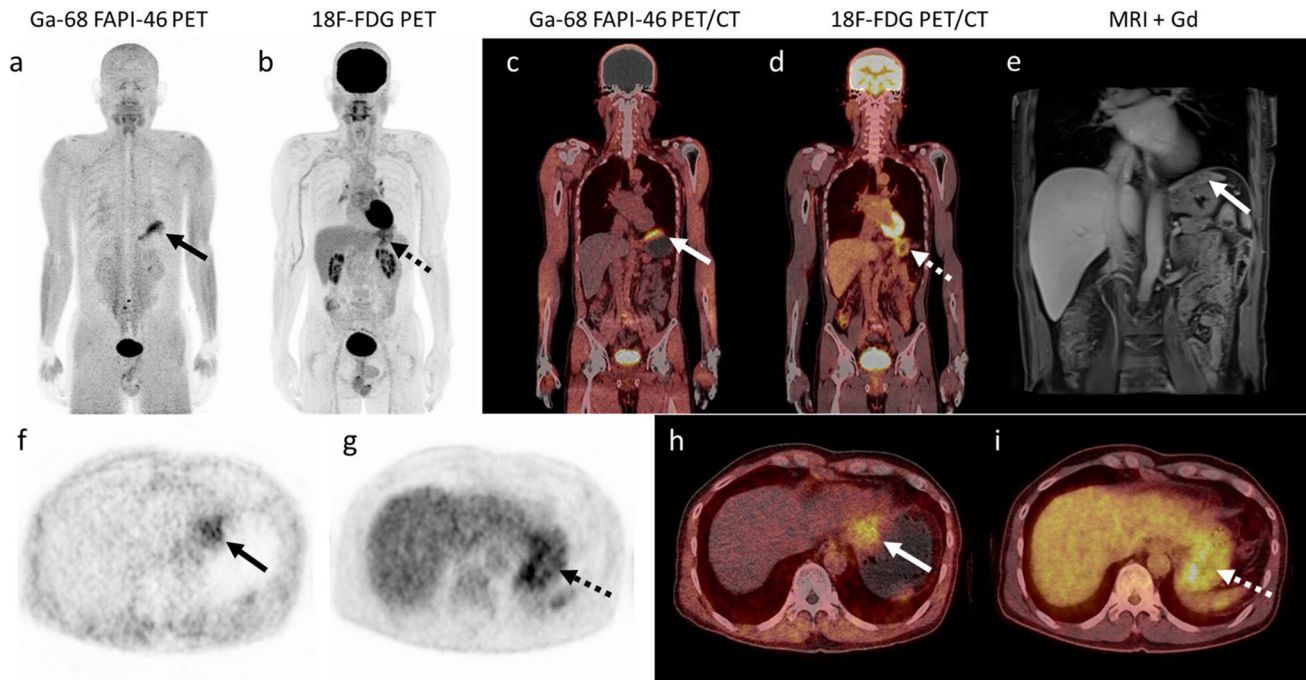


Fig. 2. A 50-year-old man with elevated AFP concentration underwent PET/CT with dedicated liver PET/MRI for diagnostic purposes. (a) MIP [⁶⁸Ga]Ga-FAPI-46 PET image, (c) coronal fused [⁶⁸Ga]Ga-FAPI-46 PET/CT image, (f) axial [⁶⁸Ga]Ga-FAPI-46 attenuation-corrected PET image, and (h) axial fused [⁶⁸Ga]Ga-FAPI-46 PET/CT image showing lesions with intense uptake (SUVmax=8.3, TBR=7.90) corresponding to the heterogeneous enhancing nodules in segment II (arrow) on (e) coronal delayed gadoxetate disodium-enhanced MRI. (b) MIP [¹⁸F]FDG PET image, (d) coronal fused [¹⁸F]FDG PET/CT image, (g) axial [¹⁸F]FDG attenuation-corrected PET image, and (i) axial fused [¹⁸F]FDG PET/CT image do not show these primary tumours because of the low level of uptake and obscuring adjacent gastric activity (arrow dot) (SUVmax=3.37, TBR=1.25).

SUV values of [¹⁸F]FDG PET/CT were lower without statistical significance ($\rho < 0.5$) in patients with CCA and HCC. The mean ADC values of hybrid PET/MR showed only low correlations ($\rho < 0.3$) with quantitative parameter values of [¹⁸F]FDG and [⁶⁸Ga]Ga-FAPI-46. Table 5 lists the results of Spearman's correlation tests between quantitative parameter values of [⁶⁸Ga]Ga-FAPI-46 PET, [⁶⁸Ga]Ga-FAPI-46 PET, and mean ADC values in patients with CCA and HCC.

Discussion

Detection Rate of [⁶⁸Ga]Ga-FAPI

Consistent with previous studies, [⁶⁸Ga]Ga-FAPI-46 PET had a high detection rate for both CCA and HCC. Moreover, [⁶⁸Ga]Ga-FAPI-46 PET was better than [¹⁸F]FDG PET/CT for identifying liver lesions. On [⁶⁸Ga]Ga-FAPI-46 PET/CT, intrahepatic tumours showed favourable tumour-to-background contrast and 100% (21/21) of patients with intrahepatic tumours were detected, a detection rate comparable with that of liver MRI (100%). In contrast, only 52% (11/21) of patients with intrahepatic tumours were

detected on [¹⁸F]FDG PET/CT. [⁶⁸Ga]Ga-FAPI-46 PET/CT showed higher activity (median SUVmax: 15.61 vs. 5.17; $P < 0.001$) and higher TBR (median, 15.90 vs. 1.69; $P < 0.001$) than [¹⁸F]FDG. These results could be because of higher primary tumour uptake of [⁶⁸Ga]Ga-FAPI-46 in comparison with [¹⁸F]FDG, and the lower hepatic background activity of [⁶⁸Ga]Ga-FAPI-46 PET.

According to previous studies, MRI has favourable diagnostic performance for intrahepatic tumour detection (100% accuracy) [11]. Thus, we used MRI as the reference standard for the diagnostic performance calculations. According to the MRI findings, there were two false-positive patients with HCC (post-treatment inflammatory processes) and no false positives among the CCA patients on [⁶⁸Ga]Ga-FAPI-46 PET/CT. Moreover, we noticed that the two false-positive patients with HCC underwent transarterial chemoembolisation. All the intrahepatic lesions detectable on MRI were also detected on [⁶⁸Ga]Ga-FAPI-46 PET/CT (100%, 19/19), whereas the sensitivity of [¹⁸F]FDG PET/CT was only 57.9% (11/19). Data from this study and previous ones show intense [⁶⁸Ga]Ga-FAPI-46 uptake caused by procedural-induced inflammation, which may be mistaken for local recurrence or residual viable tumour. Inflammation-induced nonspecific fibrosis can also lead to false-positive results; in this situation, morphological

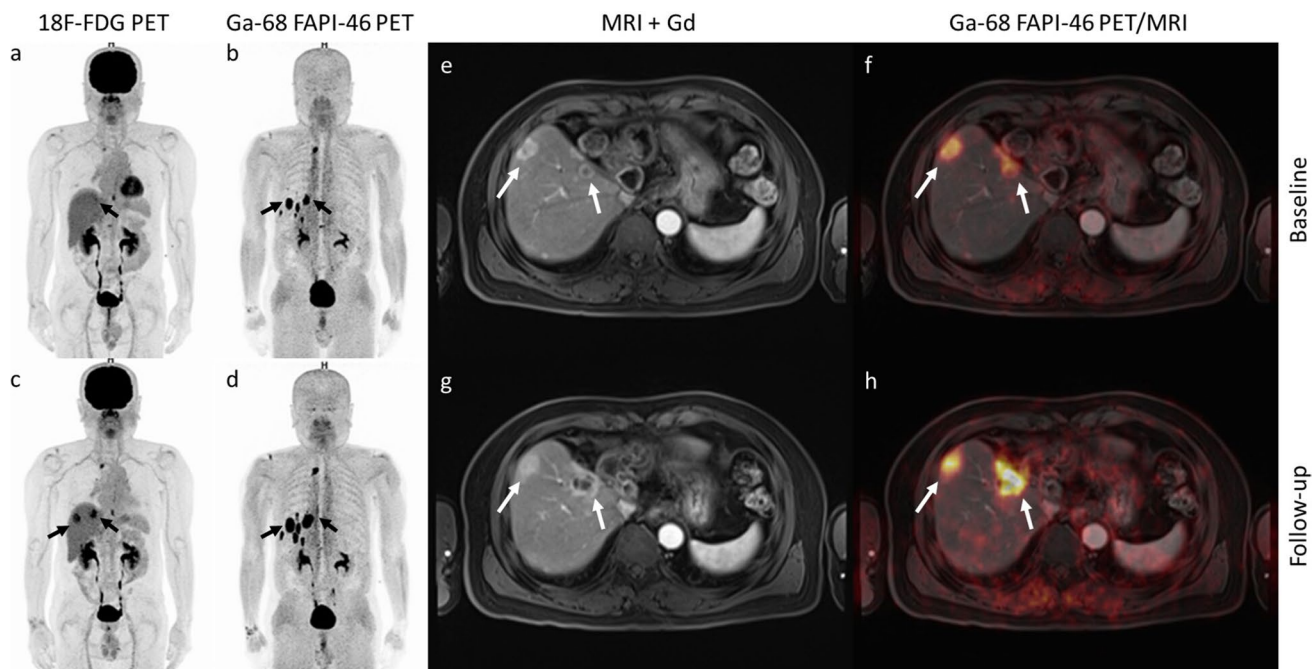


Fig. 3. A 78-year-old man with intrahepatic cholangiocarcinoma who underwent left hepatectomy and chemotherapy approximately 3 years earlier (last chemotherapy session approximately 3 months prior to imaging). The patient underwent PET/CT with dedicated liver PET/MRI for restaging. **(b)** Whole-body [⁶⁸Ga]Ga-FAPI-46 PET maximum-intensity-projection (MIP) image showing multiple intense FAPI-avid nodules (arrows) in the liver corresponding to multiple heterogeneous enhancing nodules **(e)** with fluid restriction on axial fused [⁶⁸Ga]Ga-FAPI-46 PET/MRI of the liver **(f)**; liver metastases were likely. **(a)** [¹⁸F]FDG PET MIP image showing only subtle uptake at the hepatic dome. Three months later, the patient underwent PET/CT for re-evaluation of disease: **(d)** [⁶⁸Ga]Ga-FAPI-46 PET MIP image; **(g)** axial gadolinium-enhanced MRI image; **(h)** axial fused [⁶⁸Ga]Ga-FAPI-46 PET/MRI of the liver. Follow-up [⁶⁸Ga]Ga-FAPI-46 PET/CT with dedicated liver PET/MRI shows that the previous FAPI-46-avid nodules in the residual liver have increased in size and intensity. **(c)** The paired [¹⁸F]FDG PET MIP image shows a few new FDG-avid nodules (arrows) in the liver, confirming the diagnosis of viable liver metastases in the study 3 months previous.

Table 4 Comparison of [¹⁸F]FDG and [⁶⁸Ga]Ga-FAPI-46 PET/CT in regional node metastasis and distant metastasis

Metastatic site	No. of patients	[¹⁸ F]FDG			[⁶⁸ Ga]Ga-FAPI-46		
		SUV _{max}	TBR	No. of positive lesions	SUV _{max}	TBR	No. of positive lesions
Regional nodes	12	4.61 (2.06–36.66)	2.28 (1.11–15.28)	18	8.35 (2.74–23.56)	4.51 (1.58–20.78)	31
Cervical nodes	2	6.67 (4.39–9.34)	7.10 (4.67–8.81)	3	4.74 (3.12–6.79)	3.85 (2.54–6.79)	3
Mediastinal nodes	6	6.35 (3.46–13.73)	3.14 (1.31–10.24)	13	7.31 (2.15–10.4)	5.14 (1.97–6.26)	13
Peritoneum	5	7.44 (2.97–15.96)	3.52 (1.33–14.64)	2	17.23 (6.42–35.35)	14.69 (5.05–25.80)	6
Bone	5	5.66 (3.72–8.26)	6.96 (1.31–12.49)	12	7.55 (3.1–33.59)	8.04 (4.02–22.70)	10
Lung	5	3.80 (1.39–7.13)	7.88 (0.78–25.07)	9	2.09 (1.33–27.81)	5.81 (0.98–33.41)	9
Brain	1	8.86	1.16	0	25.30	194.60	1
Muscle	1	3.49	3.60	1	8.34	5.28	1

Values are median (range)

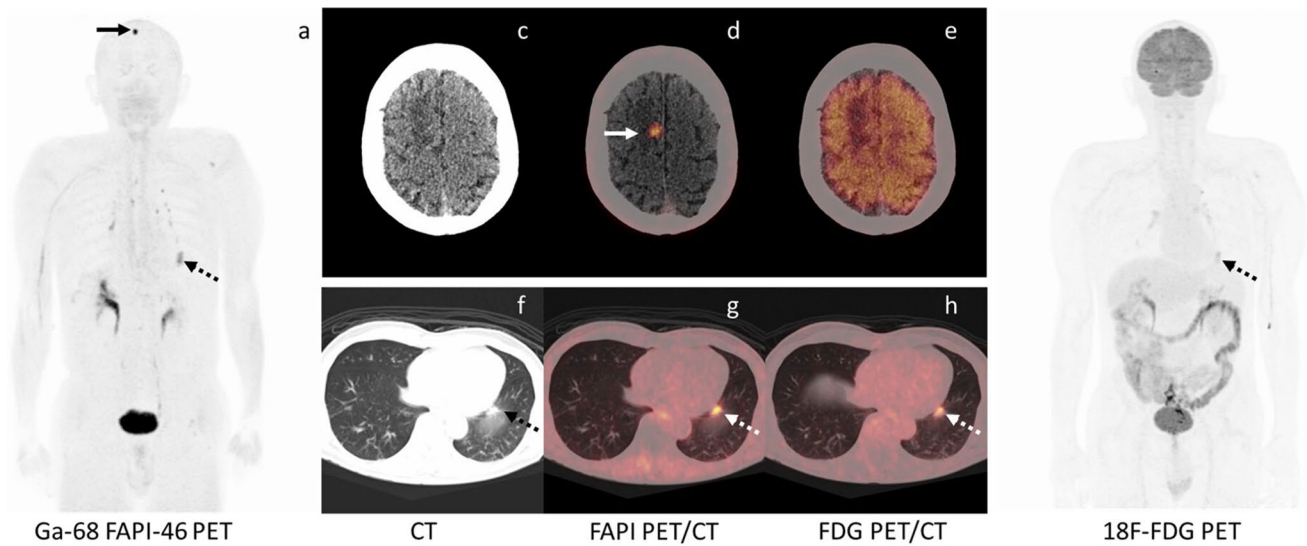


Fig. 4. A 67-year-old man with cholangiocarcinoma underwent right hepatectomy with right adrenal gland, gallbladder, and diaphragm resection approximately 1 year earlier. He also received chemotherapy (last session approximately 6 months prior to imaging) and underwent PET/CT for restaging. (a) [⁶⁸Ga]Ga-FAPI-46 PET MIP image; (c) axial conventional CT image; and (d) fused [⁶⁸Ga]Ga-FAPI-46 PET/CT images show an FAPI-avid nodule (arrow) in the right high parasagittal frontal area with perilesional brain oedema; brain metastasis was suspected and was confirmed on follow-up brain MRI. This brain metastasis was barely detectable on FDG PET. (b) FDG PET MIP image; (e) fused axial FDG PET/CT. Further brain radiotherapy treatment was scheduled. Multiple pulmonary and subpleural nodules (arrow dot) with FDG and FAPI uptake are scattered in both lungs on (a), (b), (f) axial conventional CT image; (g), fused axial [⁶⁸Ga]Ga-FAPI-46 PET/CT; and (h), fused axial FDG PET/CT.

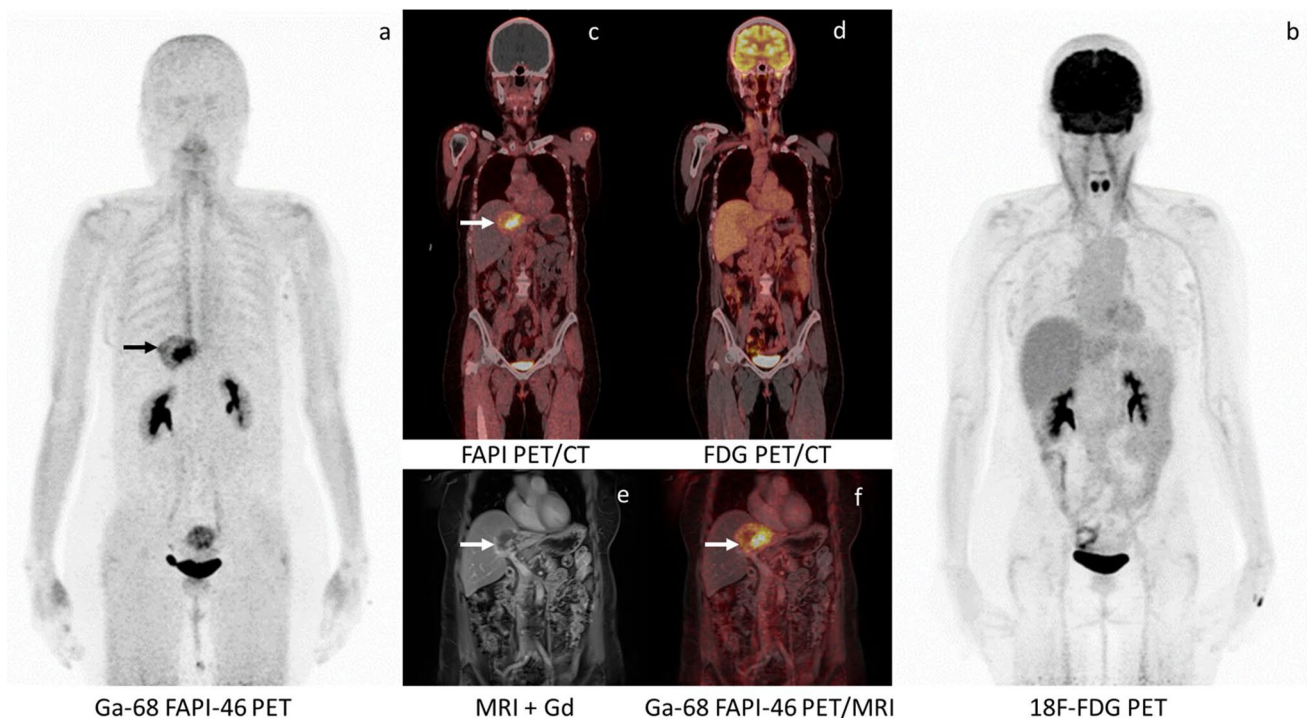


Fig. 5. Images from a 66-year-old woman with cholangiocarcinoma who underwent chemotherapy (last session approximately 3 months prior to imaging). The patient underwent PET/CT with dedicated liver PET/MRI for restaging. (a) [⁶⁸Ga]Ga-FAPI-46 PET MIP image; (c) coronal fused [⁶⁸Ga]Ga-FAPI-46 PET/CT image; (e) coronal delayed gadolinium-enhanced MRI; (f) coronal fused [⁶⁸Ga]Ga-FAPI-46 PET/MRI image. [⁶⁸Ga]Ga-FAPI-46 PET/CT images show a liver mass (arrow) with intense uptake corresponding to a peripheral gradually enhancing mass involving hepatic segments II, III, and IV on PET/MRI. (b) FDG PET MIP image and (d) coronal fused [¹⁸F]FDG PET/CT do not show the residual viable tumour, which affected this patient's management.

Table 5 Spearman’s correlation coefficients between quantitative parameter values of [⁶⁸Ga]Ga-FAPI-46 PET, [⁶⁸Ga]Ga-FAPI-46 PET, and mean ADC values in CCA and HCC

Quantitative parameter		FDG				FAPI				Rho	p value
		SUV _{max}	SUV _{mean}	SUV _{peak}	TBR	SUV _{max}	SUV _{mean}	SUV _{peak}	TBR		
CCA											
FDG	SUV _{max}	1									
	SUV _{mean}	0.942	1								
	SUV _{peak}	0.941	0.943	1							
	TBR	0.889	0.871	0.846	1						
FAPI	SUV _{max}	0.678	0.631	0.628	0.628	1					
	SUV _{mean}	0.610	0.564	0.560	0.569	0.976	1				
	SUV _{peak}	0.709	0.672	0.698	0.728	0.881	0.866	1			
	TBR	0.247	0.115	0.157	0.104	0.667	0.701	0.516	1		
ADC		0.059	0.014	0.101	0.094	0.047	0.074	-0.037	0.027		
		0.752	0.939	0.589	0.614	0.800	0.694	0.842	0.884		
HCC											
FDG	SUV _{max}	1									
	SUV _{mean}	0.957	1								
	SUV _{peak}	0.951	0.923	1							
	TBR	0.892	0.843	0.853	1						
FAPI	SUV _{max}	0.288	0.225	0.331	0.156	1					
	SUV _{mean}	0.347	0.297	0.391	0.225	0.973	1				
	SUV _{peak}	0.388	0.331	0.418	0.284	0.969	0.994	1			
	TBR	0.482	0.437	0.480	0.243	0.746	0.695	0.696	1		
ADC		0.256	0.227	0.207	0.391	0.266	0.182	0.185	0.336		
		0.304	0.364	0.410	0.109	0.286	0.470	0.462	0.173		

characteristics on MRI may help differentiate inflammatory lesions from true malignancy. Therefore, liver MRI is an important imaging modality with high specificity for the detection and characterisation of intrahepatic lesions.

Our positivity rates and sensitivities of 100% for detecting intrahepatic lesions in patients with CCA were equal to those of Shi et al. [12] and Guo et al. [11]. In contrast, the positivity rates and sensitivities for detecting intrahepatic lesions in patients with HCC were slightly higher in our study and that of Shi et al. than in the study of Guo et al. (100%, 100%, and 94%, respectively). Moreover, our median TBR and median SUVmax values, as well as those

of Shi et al., were higher than those of Guo et al. These differences might be related to different scanner technology. Cross calibration between the PET/CT and PET/MRI scanners is a key process for improving quantitative and semiquantitative parameters; it improves accuracy and provides external validity.

Metabolic tumour volume (MTV) and estimated stroma volume could not be evaluated in this study because almost half of the intrahepatic lesions showed no increased FDG uptake compared with the hepatic background, and the markedly high SUVmax of [⁶⁸Ga]Ga-FAPI-46 PET in the intrahepatic lesions affected the estimated stroma volume

measurement (which was smaller than it should have been). The low detection rate of [¹⁸F]FDG PET/CT may be related to decreased glucose transporter expression [16, 17]. Interestingly, we noted that [⁶⁸Ga]Ga-FAPI-46 uptake was higher in most CCA primary lesions than in HCC lesions, a finding that could be attributed to dense desmoplastic stroma and cancer-associated fibroblasts, which are considered hallmark histological features of cholangiocarcinoma [18–20], high expression of glucose-6-phosphatase [21], and histopathological grade, especially in HCC [5, 6, 22, 23].

One case of HCC showed a radiopharmaceutical uptake pattern that differed from the others, with the [¹⁸F]FDG uptake being greater than [⁶⁸Ga]Ga-FAPI-46 uptake, especially in bone metastases, which were false-negative on [⁶⁸Ga]Ga-FAPI-46 PET. We hypothesise that these results were related to the heterogeneity of FAP in the metastatic lesions and the histopathology of the HCC lesions.

The main advantage of [¹⁸F]FDG and [⁶⁸Ga]Ga-FAPI-46 PET over liver MRI is the detection of extrahepatic metastases. [⁶⁸Ga]Ga-FAPI-46 PET/CT revealed more positive lymph nodes and visceral metastases than [¹⁸F]FDG PET/CT, especially brain metastases and metastases in intra-abdominal (regional) and peritoneal lymph nodes. Although all patients with distant metastasis were detected on [¹⁸F]FDG and [⁶⁸Ga]Ga-FAPI-46 PET/CT imaging (100%, 14/14), [⁶⁸Ga]Ga-FAPI-46 PET detected four additional peritoneal metastases and one brain metastasis that were not detected on [¹⁸F]FDG PET, findings that affected patient management, quality of life, and prognosis. These data indicate that the use of [⁶⁸Ga]Ga-FAPI-46 PET with dedicated liver PET/MRI may improve liver cancer staging and subsequent patient management.

We are not aware of any recent reports on correlations between ADC values and quantitative parameters of [¹⁸F]FDG PET and FAPI PET in liver malignancy. Our results for intrahepatic tumours revealed that the correlations between quantitative parameter values of [⁶⁸Ga]Ga-FAPI-46 PET/CT and SUV values of [¹⁸F]FDG PET/CT were stronger in CCA than in HCC, which is possibly due to the characteristics of the primary tumours. In other words, the correlation between cancer-associated fibroblasts and glucose metabolism is stronger in CCA than in HCC.

CCA is associated with a “desmoplastic response”, or the deposition of fibrotic or connective tissue, which is usually regarded as a response to malignant cells. Formation of stroma in CCA presents as a secondary insult in response to malignant growth [24]. Cancer-associated fibroblasts promote tumour progression [20] proteins and alter the cellular architecture through overproduction of extracellular matrix [25]. [¹⁸F]FDG uptake reflects glycolytic activity which could be a prognostic indicator of aggressiveness. This knowledge suggests that FAPI PET and FDG PET might be a promising prognostic imaging workup for CCA, with their being a correlation between the tracers. However, the use of [¹⁸F]FDG PET as a prognostic imaging tool is limited by its sensitivity,

especially in small infiltrative mucinous cholangiocarcinoma and small duct cholangiocarcinoma [26–29].

Conversely, in hepatocellular carcinogenesis, cirrhosis and fibrosis generate a microenvironment that promotes tumourigenesis [24]. Most HCCs develop in fibrotic or cirrhotic livers, thereby proposing an important role of liver fibrosis in the premalignant environment of the liver [30]. Previous studies demonstrated that the gene signature of adjacent non-cancerous tissue contains key molecular information on recurrence and prognosis, illustrating that molecular prognostic determinants depend on both cancerous and non-cancerous tissue [31]. In our study, a weak correlation between cancer-related fibroblasts and glucose metabolism in HCC supports the knowledge that there is rare expression of GLUT-1 but increasing hexokinase-II expression in HCC [32, 33]. Nonetheless, prognostic imaging in HCC remains a challenge because of the limitations described above and histopathological variation.

DWI can be quantified with apparent diffusion coefficient (ADC) values and qualitatively assessed using visual analysis. Our mean ADC value for HCC was similar to that in a previous study [34]. The mean ADC values of hybrid PET/MR showed poor correlation with both desmoplastic response and glucose metabolism. This may imply that diffusion-weighted images cannot be used as a substitute for PET imaging in the specific molecular characterisation of HCC and CCA. Finally, multimodality hybrid imaging with novel radiopharmaceuticals can provide information on various aspects of cancer, resulting in a more complete biological profile.

This study has several limitations. First, this was an analysis of a heterogeneous population (patients with suspected, newly diagnosed, or previously treated liver cancer, including HCC and CCA) with a small sample size. There is a need for large-scale studies of specific cancer types. Second, pathological confirmation of nodal metastasis, distant metastasis, and local recurrent/residual tumour was not available.

Conclusion

[⁶⁸Ga]Ga-FAPI PET/CT with dedicated liver PET/MRI has superior potential for detecting hepatic malignancy than [¹⁸F]FDG PET/CT or MRI alone.

Supplementary Information The online version contains supplementary material available at <https://doi.org/10.1007/s11307-022-01732-2>.

Acknowledgements We thank SOFIE for providing the [⁶⁸Ga]Ga-FAPI-46 precursor free of charge. We thank Edanz (www.edanz.com/ac) for editing a draft of this manuscript.

Declarations

Conflict of Interest The authors declare that they have no conflict of interest.

References

- Sung H, Ferlay J, Siegel RL et al (2021) Global cancer statistics 2020: GLOBOCAN estimates of incidence and mortality worldwide for 36 cancers in 185 countries. *CA Cancer J Clin* 71:209–249. <https://doi.org/10.3322/caac.21660>
- Sripa B, Pairojkul C (2008) Cholangiocarcinoma: lessons from Thailand. *Curr Opin Gastroenterol* 24:349–356. <https://doi.org/10.1097/MOG.0b013e3282f9b3>
- Rahib L, Smith BD, Aizenberg R et al (2014) Projecting cancer incidence and deaths to 2030: the unexpected burden of thyroid, liver, and pancreas cancers in the United States. *Cancer Res* 74:2913–2921. <https://doi.org/10.1158/0008-5472.CAN-14-0155>
- Li J, Wang J, Lei L et al (2019) The diagnostic performance of gadoteric acid disodium-enhanced magnetic resonance imaging and contrast-enhanced multi-detector computed tomography in detecting hepatocellular carcinoma: a meta-analysis of eight prospective studies. *Eur Radiol* 29:6519–6528. <https://doi.org/10.1007/s00330-019-06294-6>
- Khan MA, Combs CS, Brunt EM et al (2000) Positron emission tomography scanning in the evaluation of hepatocellular carcinoma. *J Hepatol* 32:792–797. [https://doi.org/10.1016/s0168-8278\(00\)80248-2](https://doi.org/10.1016/s0168-8278(00)80248-2)
- Trojan J, Schroeder O, Raedle J et al (1999) Fluorine-18 FDG positron emission tomography for imaging of hepatocellular carcinoma. *Am J Gastroenterol* 94:3314–3319. <https://doi.org/10.1111/j.1572-0241.1999.01544.x>
- Iwata Y, Shiomi S, Sasaki N et al (2000) Clinical usefulness of positron emission tomography with fluorine-18-fluorodeoxyglucose in the diagnosis of liver tumors. *Ann Nucl Med* 14:121–126. <https://doi.org/10.1007/BF02988591>
- Huang X, Yang J, Li J, Xiong Y (2020) Comparison of magnetic resonance imaging and 18-fluorodeoxyglucose positron emission tomography/computed tomography in the diagnostic accuracy of staging in patients with cholangiocarcinoma: a meta-analysis. *Medicine (Baltimore)* 99:e20932. <https://doi.org/10.1097/MD.00000000000020932>
- Kratochwil C, Flechsig P, Lindner T et al (2019) ⁶⁸Ga-FAPI PET/CT: tracer uptake in 28 different kinds of cancer. *J Nucl Med* 60:801–805. <https://doi.org/10.2967/jnumed.119.227967>
- Chen H, Pang Y, Wu J et al (2020) Comparison of [⁶⁸Ga]Ga-DOTA-FAPI-04 and [¹⁸F]FDG PET/CT for the diagnosis of primary and metastatic lesions in patients with various types of cancer. *Eur J Nucl Med Mol Imaging* 47:1820–1832. <https://doi.org/10.1007/s00259-020-04769-z>
- Guo W, Pang Y, Yao L et al (2021) Imaging fibroblast activation protein in liver cancer: a single-center post hoc retrospective analysis to compare [⁶⁸Ga]Ga-FAPI-04 PET/CT versus MRI and [¹⁸F]-FDG PET/CT. *Eur J Nucl Med Mol Imaging* 48:1604–1617. <https://doi.org/10.1007/s00259-020-05095-0>
- Shi X, Xing H, Yang X et al (2021) Comparison of PET imaging of activated fibroblasts and 18F-FDG for diagnosis of primary hepatic tumours: a prospective pilot study. *Eur J Nucl Med Mol Imaging* 48:1593–1603. <https://doi.org/10.1007/s00259-020-05070-9>
- Lindner T, Loktev A, Altmann A et al (2018) Development of quinoline-based theranostic ligands for the targeting of fibroblast activation protein. *J Nucl Med* 59:1415–1422. <https://doi.org/10.2967/jnumed.118.210443>
- Loktev A, Lindner T, Mier W et al (2018) A tumor-imaging method targeting cancer-associated fibroblasts. *J Nucl Med* 59:1423–1429. <https://doi.org/10.2967/jnumed.118.210435>
- Boonkawin N, Chotipanich C (2021) The first radiolabeled ⁶⁸Ga-FAPI-46 for clinical PET applications using a fully automated iQS-TS synthesis system in Thailand. *J Chulabhorn Royal Acad* 3:180–188
- Zimmerman RL, Burke M, Young NA et al (2002) Diagnostic utility of Glut-1 and CA 15–3 in discriminating adenocarcinoma from hepatocellular carcinoma in liver tumors biopsied by fine-needle aspiration. *Cancer* 96:53–57. <https://doi.org/10.1002/cncr.10309.abs>
- Lee JD, Yang WI, Park YN et al (2005) Different glucose uptake and glycolytic mechanisms between hepatocellular carcinoma and intrahepatic mass-forming cholangiocarcinoma with increased (18)F-FDG uptake. *J Nucl Med* 46:1753–1759
- Mertens JC, Rizvi S, Gores GJ (2018) Targeting cholangiocarcinoma. *Biochim Biophys Acta Mol Basis Dis* 1864:1454–1460. <https://doi.org/10.1016/j.bbadis.2017.08.027>
- Coulouarn C, Clément B (2014) Stellate cells and the development of liver cancer: therapeutic potential of targeting the stroma. *J Hepatol* 60:1306–1309. <https://doi.org/10.1016/j.jhep.2014.02.003>
- Sirica AE (2011) The role of cancer-associated myofibroblasts in intrahepatic cholangiocarcinoma. *Nat Rev Gastroenterol Hepatol* 9:44–54. <https://doi.org/10.1038/nrgastro.2011.222>
- Torizuka T, Tamaki N, Inokuma T et al (1995) In vivo assessment of glucose metabolism in hepatocellular carcinoma with FDG-PET. *J Nucl Med* 36:1811–1817
- Hu J-H, Tang J-H, Lin C-H et al (2018) Preoperative staging of cholangiocarcinoma and biliary carcinoma using 18F-fluorodeoxyglucose positron emission tomography: a meta-analysis. *J Investig Med* 66:52–61. <https://doi.org/10.1136/jim-2017-000472>
- Lee Y, Yoo IR, Boo SH et al (2017) The role of F-18 FDG PET/CT in intrahepatic cholangiocarcinoma. *Nucl Med Mol Imaging* 51:69–78. <https://doi.org/10.1007/s13139-016-0440-y>
- Lee JJ, Campbell JS (2014) Role of desmoplasia in cholangiocarcinoma and hepatocellular carcinoma. *J Hepatol* 61:432–434. <https://doi.org/10.1016/j.jhep.2014.04.014>
- Blaauboer ME, Boeijen FR, Emson CL et al (2014) Extracellular matrix proteins: a positive feedback loop in lung fibrosis? *Matrix Biol* 34:170–178. <https://doi.org/10.1016/j.matbio.2013.11.002>
- Anderson CD, Rice MH, Pinson CW et al (2004) Fluorodeoxyglucose PET imaging in the evaluation of gallbladder carcinoma and cholangiocarcinoma. *J Gastrointest Surg* 8:90–97. <https://doi.org/10.1016/j.gassur.2003.10.003>
- Fritscher-Ravens A, Bohuslavizki KH, Broering DC et al (2001) FDG PET in the diagnosis of hilar cholangiocarcinoma. *Nucl Med Commun* 22:1277–1285. <https://doi.org/10.1097/00006231-200112000-00002>
- Petrowsky H, Wildbrett P, Husarik DB et al (2006) Impact of integrated positron emission tomography and computed tomography on staging and management of gallbladder cancer and cholangiocarcinoma. *J Hepatol* 45:43–50. <https://doi.org/10.1016/j.jhep.2006.03.009>
- Kozaka K, Kobayashi S, Takamura H et al (2020) Differences in 18F-FDG uptake and expression of glucose transporter between 2 distinct subtypes of mass-forming intrahepatic cholangiocarcinomas. *Clin Nucl Med* 45:e267–e273. <https://doi.org/10.1097/RLU.0000000000003055>
- Affo S, Yu L-X, Schwabe RF (2017) The role of cancer-associated fibroblasts and fibrosis in liver cancer. *Annu Rev Pathol* 12:153–186. <https://doi.org/10.1146/annurev-pathol-052016-100322>
- Hoshida Y, Villanueva A, Kobayashi M et al (2008) Gene expression in fixed tissues and outcome in hepatocellular carcinoma. *N Engl J Med* 359:1995–2004. <https://doi.org/10.1056/NEJMoa0804525>
- Zimmerman RL, Fogt F, Burke M, Murakata LA (2002) Assessment of Glut-1 expression in cholangiocarcinoma, benign biliary lesions and hepatocellular carcinoma. *Oncol Rep* 9:689–692
- Mathupala SP, Rempel A, Pedersen PL (1995) Glucose catabolism in cancer cells. Isolation, sequence, and activity of the promoter for type II hexokinase. *J Biol Chem* 270:16918–16925. <https://doi.org/10.1074/jbc.270.28.16918>
- Shankar S, Kalra N, Bhatia A et al (2016) Role of diffusion weighted imaging (DWI) for hepatocellular carcinoma (HCC) detection and its grading on 3T MRI: a prospective study. *J Clin Exp Hepatol* 6:303–310. <https://doi.org/10.1016/j.jceh.2016.08.012>